Spectroscopic properties of thulium ions in bismuth silicate glass

Xin Wang (王 欣)[1,2*], Lili Hu (胡丽丽)[1], Kefeng Li (李科峰)[1], Ying Tian (田 颖)[1,2], and Sijun Fan (凡思军)[1,2]

[1]*Shanghai Institute of Optics and Fine Mechanics, Chinese Academy of Science, Shanghai 201800, China*

[2]*Graduate Universitiy of Chinese Academy of Science, Beijing 100049, China*

[*]*Corresponding author: mijinsan@163.com*

Received February 9, 2012; accepted April 13, 2012; posted online August 16, 2012

A new type of bismuth silicate glass (Bi_2O_3-SiO_2-ZnO-Al_2O_3-La_2O_3) doped with Tm_2O_3 is prepared by melt-quenching method. The thermal stability of the glass is examined by differential scanning calorimetry. No crystallization peak is found. Using the absorption and emission spectra, the absorption and emission cross-sections are calculated. Their maximum data are 2.9×10^{-21} cm^2 at 1 663 nm and 4.7×10^{-21} cm^2 at 1 826 nm, respectively. Using the Judd-Ofelt theory, the radiation transition probabilities and radiative lifetimes are obtained. The extended overlap integral method is applied to analyze energy transfer process among the Tm^{3+} ions. The transfer constants of cross-relaxation and energy migration among the Tm^{3+}ions at the $^3H_4$ level are 7.60×10^{-40} and 14.98×10^{-40} cm^6/s, respectively. The critical transfer radius for cross-relaxation is 0.99 nm. The cross relaxation process is easy to realize and is favorable for obtaining ~2-μm laser.

OCIS codes: 160.2290, 160.2750, 160.3380, 160.5690, 160.4670.

doi: 10.3788/COL201210.101601.

In recent years, much attention has been paid to eye-safe ~2-μm lasers due to their important applications, such as in mid-infrared remote sensing, light detection and ranging, laser medical applications, and pumping parametric oscillators[1−4]. Because strong fluorescence in the broad range from 1.6 to 1.9 μm can be obtained using Tm^{3+} as an active ion due to the $^3F_4 \rightarrow {}^3H_6$ transition, many types of thulium-doped glasses have been investigated to realize ~2-μm lasers[3,5−9]. Compared with other glasses, silicate glasses have relatively low thermal expansion coefficients, excellent mechanical characteristics, and high solubility for rare earth ions, which are favorable for optical applications. However, silicate glasses usually have relatively high phonon energy, which leads to harmful nonradiative transition. Bismuthate glasses have low phonon energy[10] and can be easily combined with silicate glasses. Therefore, bismuth silicate glasses may have good physical and chemical properties, similar to normal silicate glasses. To develop more efficient optical devices based on Tm^{3+}, the host glass and the concentration of Tm^{3+} are two important issues to be considered.

In this letter, Bi_2O_3-SiO_2-ZnO-Al_2O_3-La_2O_3 (BSZAL) glass is chosen as host, and the infrared emission properties of Tm^{3+}-doped BSZAL glasses with Tm_2O_3 concentrations ranging from 0.1 mol% to 1.5 mol% are characterized. The curve of differential scanning calorimetry (DSC) and thermal expansion coefficient is plotted to investigate the thermal stability of the glass. Absorption and emission spectra are tested to calculate the absorption and emission cross-sections. In addition, the Judd-Ofelt parameters, spontaneous transition probability, and radiative lifetime of excited levels are calculated from the absorption spectra. The microscopic parameters of the energy transfer process are calculated using the extended overlap integral method.

Bismuth silicate glasses with mol% compositions of 15Bi_2O_3-50SiO_2-10ZnO-15Al_2O_3-10La_2O_3-$x$$Tm_2O_3$ (where x=0.1, 0.25, 0.5, 0.75, 1, 1.25, and 1.5 mol %), hereafter named as BSZAL1 to BSZAL7, are prepared by melt-quenching method. The chemicals used (together with their purities) are as follows: Bi_2O_3(99%), SiO_2(99%), ZnO(99.9%), Al_2O_3(99.9%), La_2O_3(99.9%), Tm_2O_3(99.95%). Mixed-power batches in corundum crucibles are melted in SiC-resistance electric furnace at 1 350 °C for 30 min. Then, the melts are poured on a preheated steel molds and annealed in a furnace near the glass-transition temperature for a minimum of 2 h. All annealed samples are fabricated to a polished plane parallel glass of 1-mm thickness for optical measurements.

The refractive index of the host at 1 552 nm is measured by the prism minimum deviation method, whereas the density is measured by the Archimedes water-immersion method in distilled water. The coefficient of thermal expansion is measured using a NETZSCH 402EP with a heating rate of 10 °C/min. The DSC curve is recorded by NETZSCH STA 409PC. The absorption spectra are recorded with a spectrophotometer (Lambda 900UV-vis-NIR Perklin-Elmer, USA). The emission spectra are measured with a spectrometer (Traix 320, Jobin-Yvon Co., France) using a 794-nm laser diode as an excitation source. For the lifetime measurements using a pulsed laser at 794 nm, the instrument applied is an FLSP 920 (Edinburgh instrument Ltd, UK). All the measurements are performed at room temperature.

The refractive index of the host glass is 1.80, and the glass density is 5.0 g/cm^3. Figure 1 shows the thermal property of BSZAL glass. From the DSC curve of this glass, no crystallization peak is apparent, and the glass transformation temperature T_g is 660 °C. The thermal expansion coefficient is 6.2×10^{-6}/°C, with the initial softening temperature of 739 °C. From the data of DSC

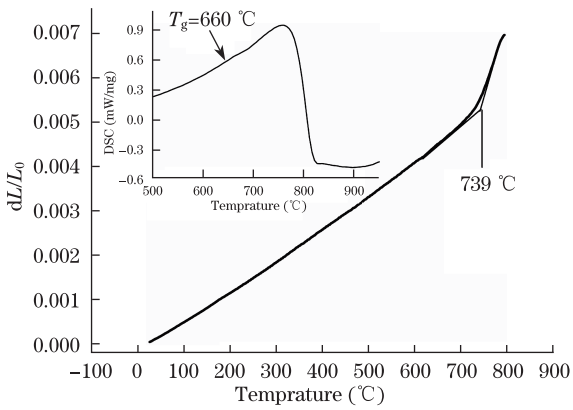

Fig. 1. Thermal property of BSZAL glass.

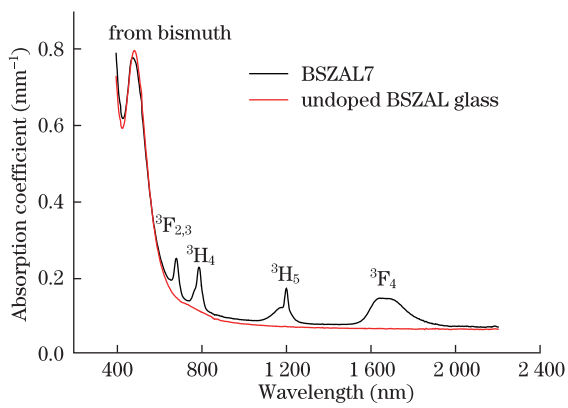

Fig. 2. Absorption spectra of Tm^{3+}-doped and undoped BSZAL glasses.

and the thermal expansion coefficient, we could conclude that thermal properties of the BSZAL glass are good for fiber drawing.

The absorption spectra of both the Tm^{3+}-doped BSZAL7 and undoped BSZAL glasses obtained at room temperature are shown in Fig. 2. The absorption spectra of the low doping concentration samples, which are similar to those of BSZAL7, are not shown for brevity. Four absorption peaks at 684, 790, 1 202, and 1 648 nm are observed. The corresponding absorptions from the ground energy level $^3H_6$ to the excited energy level $^3F_{2,3}$, $^3H_4$, $^3H_5$ and $^3F_4$ are labeled. In addition to the absorption peaks from rare earth ions, a peak is present at 490 nm, which may have originated from the absorption of bismuth[11]. Because of the effect of Bi absorption in 490 nm, the weak absorption from $^3H_6$ to $^1G_4$ of Tm^{3+} ion near 460 nm cannot be clearly identified.

The Judd-Ofelt parameters can be obtained using the data of absorption spectra, refractive index, and density[12,13]. These data, together with those of other glasses, are listed in Table 1. Here, Ω_2 is sensitive to the local environment of the rare earth ions and is dependent upon the symmetry of the coordination structure, the polarizability of the ligand ions, and the bonding nature. A large Ω_2 means a low symmetry of the ligand, a strong polarizability of the anion, and strong covalent bonding of the rare earth ions with the ligand ions[14,15]. Because the electronegativity of fluorine is bigger than that of oxide, Ω_2 of fluoride glass is smaller than that of oxide glass. Here, Bi^{3+} has a large polarizing effect on the anions, leading to an increase of covalency between Bi^{3+} and the oxygen ions, which results in smaller covalency between Tm^{3+} and oxygen ions. Thus, the Ω_2 of BSZAL is smaller than those of other oxide glasses. In contrast, Ω_4 and Ω_6 are related to the rigidity and 6-s electron density of the rare earth ions[16], with Ω_4/Ω_6 representing the spectroscopic quality of material[17]. Among all glasses in Table 1, the present BSZAL glass shows the highest Ω_4/Ω_6, indicating desirable performance. The ions at the $^3H_4$ energy level have larger probability to $^3H_5$ or $^3F_4$ than $^3H_4$, which could be deduced from the reduced matrix elements[18].

Using the Judd-Ofelt parameters, the theoretical values of the transition probability, branching ratio, and radiative lifetime can be calculated by the method in Ref. [19]. The results of the BSZAL glasses are shown in Table 2. The transition probability from $^3F_4$ to $^3H_6$ is 311.7 s^{-1}. As shown in Table 3, this value is higher than the one for fluoride, germanate, phosphate, silicate, and fluorophosphate glasses, but smaller than that for tellurite glass[20,21], which shows that the transition probability relates to refractive index; a bigger refractive index leads to a larger transition probability.

The absorption and stimulated emission cross-sections were calculated by Beer-Lambert and McCumber theory for the Tm^{3+} ions as[10,22]

$$\sigma_{\rm abs} = \frac{2.303\log[I_0(\lambda)/I(\lambda)]}{Nl}, \quad (1)$$

$$\sigma_{\rm ems} = \sigma_{\rm abs}\frac{Z_{\rm l}}{Z_{\rm u}}\exp\left[\frac{hc}{kT}\left(\frac{1}{\lambda_{\rm ZL}}-\frac{1}{\lambda}\right)\right], \quad (2)$$

Table 1. Judd-Ofelt Parameters of Various Glasses

Host Glass	Ω_2 ($\times10^{-20}$ cm^2)	Ω_4 ($\times10^{-20}$ cm^2)	Ω_6 ($\times10^{-20}$ cm^2)	Ω_4/Ω_6	Reference
ZBLAN	1.96	1.36	1.16	1.17	[18]
Germanate	5.55	2.03	1.26	1.61	[29]
Tellurite	4.09	1.36	1.19	1.14	[21]
Fluorophosphate	3.01	2.56	1.54	1.66	[19]
Bismuthate	4.35	1.49	0.96	1.55	[10]
Silica	6.23	1.91	1.36	1.40	[18]
BSZAL	2.97	1.52	0.94	1.61	this work

Table 2. Spectroscopic Parameters of Tm^{3+}-doped BSZAL Glass Calculated from Judd-Ofelt Theory

Transition	λ (nm)	A_{ed} (s^{-1})	A_{md}(s^{-1})	β (%)	τ_r (μs)
$^3F_{2,3} \rightarrow {}^3H_4$	5 098	5.7	0	0.1	231.3
$^3F_{2,3} \rightarrow {}^3H_5$	1 587	339.5	0	7.9	
$^3F_{2,3} \rightarrow {}^3F_4$	1 169	117.9	85.8	4.7	
$^3F_{2,3} \rightarrow {}^3H_6$	684	3 774.4	0	87.3	
$^3H_4 \rightarrow {}^3H_5$	2 305	28.6	13.9	2.1	505.8
$^3H_4 \rightarrow {}^3F_4$	1 517	123.9	0	6.3	
$^3H_4 \rightarrow {}^3H_6$	790	1 811.0	0	91.6	
$^3H_5 \rightarrow {}^3F_4$	4 442	9.3	0	1.9	1 991.3
$^3H_5 \rightarrow {}^3H_6$	1 202	396.8	96.1	98.1	
$^3F_4 \rightarrow {}^3H_6$	1 648	311.7	0	100	3 208.6

Table 3. Transition Probability from $^3F_4$ to $^3H_6$ Transition and Max Emission Cross-Section

	A (s^{-1})	σ_{ems} ($\times 10^{-21}$ cm^2)
Fluoride[20]	115.0	3.2
Fluorophosphates[20]	153.7	4.3
Tellirate[21]	558.7	4.0
Germanate[20]	200.5	6.8
Silicate[20]	201.6	8.4
This work	311.7	4.7

where σ_{abs} represents the absorption cross-section, $I_0(\lambda)$ and $I(\lambda)$ are the incident and outgoing light intensities through the samples, respectively, N is rare earth ion concentration, l is thickness of the sample, σ_{ems} is the emission cross-section, T is the room temperature, and k is the Boltzmann constant. In addition, Z_l and Z_u are the partition functions for the lower and upper levels, respectively, and λ_{ZL} is wavelength corresponding to the zero line energy, which is the difference between the lowest stark multiples of up and low energy level. Using the method in Ref. [23], we calculate that Z_l/Z_u is equal to 1.32 and λ_{ZL} is 1 721.8 nm.

The calculated absorption and emission cross-sections are shown in Fig. 3. The max emission cross-section by McCumber method is 0.47×10^{-20} cm^2 (at 1 826 nm), whereas the max absorption cross-section is 0.29×10^{-20} cm^2 (at 1 663 nm). As shown in Table 3, the max emission cross-section of the Tm^{3+} ion in the BSZAL glass is

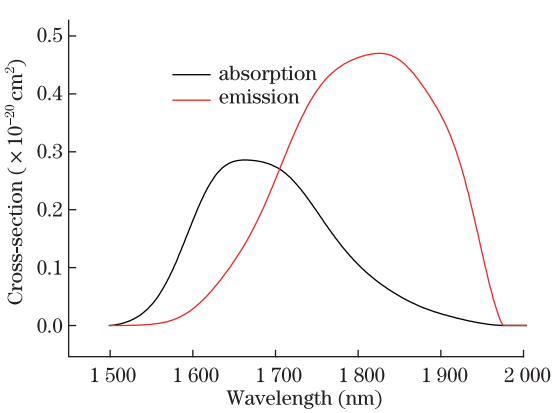

Fig. 3. Absorption and emission cross-sections of Tm^{3+}-doped BSZAL glass.

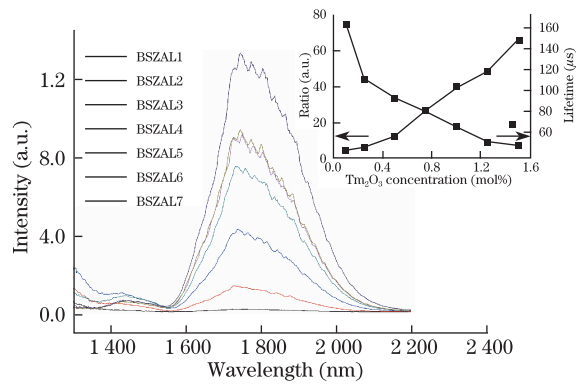

Fig. 4. Emission spectra of BSZAL glasses with different Tm_2O_3 contents. The inset shows the ratios of the $^3H_4 \rightarrow {}^3F_4$ emission intensities to the $^3F_4 \rightarrow {}^3H_6$ emission intensities and the lifetime of the $^3H_4$ level.

larger than that of the fluoride[20], fluorophosphate[20], and tellirate[21] glasses, but smaller than that of the germanate and silicate ($50SiO_2$-$5AlO_{1.5}$-$24LiO_{0.5}$-$12NaO_{0.5}$-9SrO) glasses [20]. The large value indicates that the Tm^{3+}-doped BSZAL glass is a promising material for ~2-μm amplifiers and lasers.

The emission spectra of the BSZAL glasses with different Tm_2O_3 contents are shown in Fig. 4. As the Tm_2O_3 content increases, the emission intensity of the $^3H_4 \rightarrow {}^3F_4$ transition drops, whereas that of the $^3F_4 \rightarrow {}^3H_6$ transition is enhanced. The ratio of emission intensities between the $^3H_4 \rightarrow {}^3F_4$ to $^3F_4 \rightarrow {}^3H_6$ transition and the lifetime of the $^3H_4$ level are given in the inset. As the Tm_2O_3 concentration increases, the distance between the Tm^{3+} ions at the $^3H_4$ and $^3H_6$ levels decrease, and the ion at the $^3H_4$ level more easily relaxes to the $^3F_4$ level while exciting the ion at the $^3H_6$ level to the $^3F_4$ level. Thus, this process, usually called cross-relaxation, reduces the number of ions at the $^3H_4$ level and increases the ions at the $^3F_4$ energy level, resulting in the rise of emission intensity ratio and decrease of lifetime as the Tm_2O_3 concentration increases. The energy diagram obtained from the absorption spectra is shown in Fig. 5. The cross-relaxation (CR) ($^3H_4$+$^3H_6$$\rightarrow$$^3F_4$+$^3F_4$) and energy migration (EM) ($^3H_4$+$^3H_6$$\rightarrow$$^3H_6$+$^3H_4$) processes of the Tm^{3+} ions are also indicated. Because the theoretical quantum efficiency of the cross-relaxation is 200%, which is favorable for the ~2-μm emission, we need to analyze those processes to obtain the energy trans-

fer microscopic parameters. The extended overlap integral method has been widely used in analyzing donor–accepter energy transfer processes[22,24,25]. The microscopic energy transfer probability rate between donor and acceptor ions concerning a dipole–dipole interaction can be expressed as [22]

$$W_{\mathrm{D-A}}(R) = \frac{C_{\mathrm{D-A}}}{R^6}, \tag{3}$$

where R is the distance between donor and acceptor, and $C_{\mathrm{D-A}}$ is the transfer constant (cm^6/s) defined as[26]

$$C_{\mathrm{D-A}} = \frac{R_{\mathrm{C}}^6}{\tau_{\mathrm{D}}}, \tag{4}$$

where R_{C} is the critical radius of the interaction and τ_{D} is the intrinsic lifetime-of-the-donor excited level. If we consider the phonon participated process, the transfer constant can be expressed as[22,25]

$$C_{\mathrm{D-A}} = \frac{6cg_{\mathrm{low}}^{\mathrm{D}}}{(2\pi)^4 n^2 g_{\mathrm{up}}^{\mathrm{D}}} \sum_{m=0}^{\infty} \mathrm{e}^{-(2\overline{n}+1)S_0} (\overline{n}+1)^m \cdot \int \sigma_{\mathrm{ems}}^{\mathrm{D}}(\lambda_{\mathrm{m}}^{+}) \sigma_{\mathrm{ab}}^{A}(\lambda) \mathrm{d}\lambda, \tag{5}$$

where c is the light speed, n is the refractive index, $g_{\mathrm{low}}^{\mathrm{D}}/g_{\mathrm{up}}^{\mathrm{D}}$ is the degeneracy of the respective lower and upper levels of the donor, $\overline{n} = 1/(\mathrm{e}^{\hbar\omega_0/kT} - 1)$ is the average number of phonons of energy $\hbar\omega_0$ at temperature T, m is number of the phonons that participate the energy transfer, S_0 is the Huang-Rhys factor (which is 0.31 for Tm[24]), $\lambda_m^+ = 1/(1/\lambda - m\hbar\omega_0)$ is the wavelength with m phonon creation, and $\hbar\omega_0$ is the max phonon energy, which is 920 cm^{-1} for the BSZAL glass measured by Raman spectra, as shown in the inset of Fig. 6. The max phonon energy of the BSZAL glass is smaller than that (1 050 cm^{-1}) of the silicate glass in Ref. [20], which means longer lifetime of the $^3\mathrm{F}_4$ level in the BSZAL glass (1.11 ms for the BSZAL1 glass, as seen in Fig. 6, compared with 0.25 ms for the glass in Ref. [20]) because of lower multi-phonon relaxation. The cross-sections used in the calculation and energy diagram are shown in Fig. 5.

Table 4 shows the phonon numbers, contribution terms to the total probability in energy transfer, the transfer constant, and the critical radius. Considering the contribution terms, we can conclude that one phonon is needed to achieve the cross-relaxation ($^3\mathrm{H}_6 + {}^3\mathrm{H}_4 \rightarrow {}^3\mathrm{F}_4 + {}^3\mathrm{F}_4$); however, the energy migration process ($^3\mathrm{H}_6 + {}^3\mathrm{H}_4 \rightarrow {}^3\mathrm{H}_4 + {}^3\mathrm{H}_6$) is quasi-resonant. The transfer constant for EM is much larger than that for CR. The ratio is nearly 2 because of the quasi-resonant mechanism for the EM process. The value of the critical radius for CR in the BSZAL glass is 0.99 nm, which is larger than the reported value for the tellurite (0.83 nm) [21] and chalcogenide (0.73 nm)[27], smaller than the one for the fluoride (1.79 nm)[28], and close to that for the germanate (1.08 nm) glasses[26]. Larger critical radius means higher efficiency to realize the cross-relaxation process; thus, a large critical radius is needed in order to realize the ∼2-μm laser of Tm^{3+}.

In conclusion, bismuth silicate glass ($\mathrm{Bi_2O_3}$-$\mathrm{SiO_2}$-ZnO-$\mathrm{Al_2O_3}$-$\mathrm{La_2O_3}$) with good thermal properties is obtained using the melt-quenching method. From the absorption

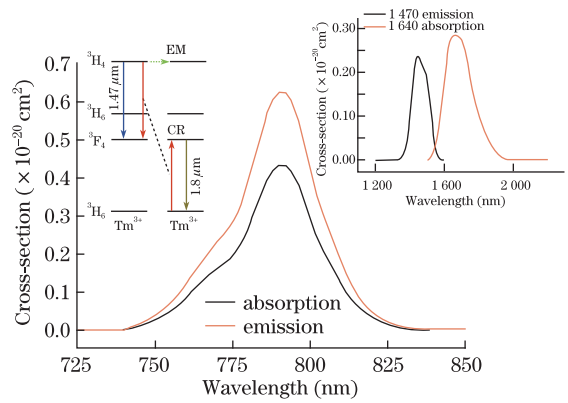

Fig. 5. Cross-section of Tm^{3+}-doped BSZAL glass between the $^3\mathrm{H}_4$ and $^3\mathrm{H}_6$ levels. The inset at left is the energy level and the energy transfer process diagram; the inset at right is the emission cross-section at 1 470 nm and absorption cross-section at 1 663 nm.

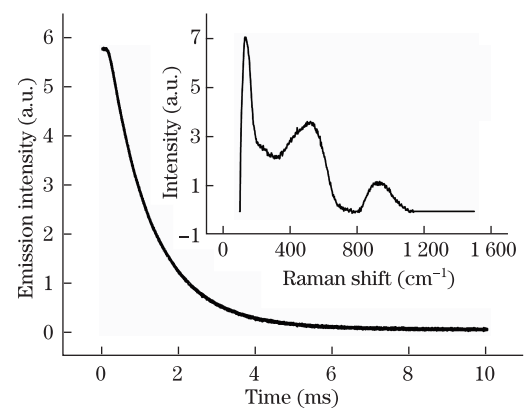

Fig. 6. Fluorescent lifetime of BSZAL1 glass. The inset shows Raman spectra of BSZAL glass.

Table 4. Energy Transfer Constants, Critical Radius, and Contribution Terms of Phonons During the Energy Transfer Process

Energy Transfer	PN-CT	$C_{\mathrm{D-A}}$ ($\times 10^{-40}\mathrm{cm}^6/\mathrm{s}$)	R_{C} (nm)
CR($^3\mathrm{H}_6 + {}^3\mathrm{H}_4 \rightarrow {}^3\mathrm{F}_4 + {}^3\mathrm{F}_4$)	0-2%	0.99	
	1-93%		
	2-5%		
EM($^3\mathrm{H}_6 + {}^3\mathrm{H}_4 \rightarrow {}^3\mathrm{F}_4 + {}^3\mathrm{F}_4$)	0-99%	14.98	1.11
	1-1%		

Phonom number (PN); contribution term (CT).

spectra, the Judd-Ofelt parameters are calculated, revealing the Ω_2, Ω_4, and Ω_6 values to be 2.97×10^{-20}, $1.52\times10^{-20,}$ and 2.97×10^{-20} cm^2. The absorption cross-section is calculated using the Beer-Lambert method. The peak value is 0.29×10^{-20} cm^2 at 1 663 nm. The max emission cross-section from McCumber is 0.47×10^{-20} cm^2 at 1 826 nm. The lifetime of the $^3F_4$ energy level in the low-Tm^{3+}-doped sample is 1.1 ms. As the doping concentration increases, the probability of cross-relaxation rises, whereas the ratio of emission intensities of $^3H_4\rightarrow{}^3F_4$ to $^3F_4\rightarrow{}^3H_6$ transition and lifetime of $^3H_4$ energy level decrease. An extended method based on extended overlap integral method is used to analyze the energy transfer process, during which the cross-relaxation and energy migration are considered. The transfer constants for cross-relaxation and energy migration processes are 7.60×10^{-40} and 14.98×10^{-40} cm^6/s. The big critical radius (0.99 nm) for the cross-relaxation process means it could work easily and it is favorable for realizing the ~2-μm laser.

This work was supported by the National Natural Science Foundation of China (No. 60937003) and GF foundation (No. GXJJ-11-M23).

References

1. B. M. Walsh, Laser Phys. **19,** 855 (2009).
2. J. Wu, Z. Yao, J. Zong, A. Chavez-Pirson, N. Peyghambarian, and J. Yu, Proc. SPIE **7195,** 71951K (2009).
3. J. Shibin, in *Proceedings of Conference of OFC/NFOEC* OMQ4 (2011).
4. R. Zhou, Y. Ju, Y. Zhang, and Y. Wang, Chin. Opt. Lett. **9,** 071401 (2011).
5. P. Zhao, J. Liu, C. Zhao, H. Yang, and J. Wen, Proc. SPIE **7843,** 784306 (2010).
6. N. P. Barnes, B. M. Walsh, D. J. Reichle, R. J. Deyoung, and S. B. Jiang, Appl. Phys. B **89,** 299 (2007).
7. J. F. Wu, S. B. Jiang, T. Luo, J. H. Geng, N. Peyghambarian, and N. P. Barnes, IEEE Photon. Technol. Lett. **18,** 334 (2006).
8. J. Geng, Q. Wang, T. Luo, S. Jiang, and F. Amzajerdian, Opt. Lett. **34,** 3493 (2009).
9. K. Li, G. Zhang, and L. Hu, Opt. Lett. **35,** 4136 (2010).
10. H. Fan, G. Gao, G. Wang, J. Hu, and L. Hu, Opt. Mater. **32,** 627 (2010).
11. B. Denker, B. Galagan, V. Osiko, I. Shulman, S. Sverchkov, and E. Dianov, Appl. Phys. B **95,** 801 (2009).
12. Y. Nageno, H. Takebe, and K. Morinaga, J. Am. Ceramic Soc. **76,** 3081 (1993).
13. B. R. Judd, Phys. Rev. **127,** 750 (1962).
14. K. Annapurna, M. Das, and S. Buddhudu, Phys. B **388,** 174 (2007).
15. S. Tanabe, T. Ohyagi, S. Todoroki, T. Hanada, and N. Soga, J. Appl. Phys. **73,** 8451 (1993).
16. P. S. Golding, S. D. Jackson, T. A. King, and M. Pollnau, Phys. Rev. B **62,** 856 (2000).
17. P. R. Watekar, S. Ju, S. Boo, and W.-T. Han, J. Non-Cryst. Solids **351,** 2446 (2005).
18. B. M. Walsh and N. P. Barnes, Appl. Phys. B **78,** 325 (2004).
19. Y. Tian, R. R. Xu, L. Y. Zhang, L. L. Hu, and J. J. Zhang, J. Appl. Phys. **108,** 083504 (2010).
20. B. Peng and T. Izumitani, Opt. Mater. **4,** 797 (1995).
21. R. Balda, J. Fernandez, S. Garcia-Revilla, and J. M. Fernandez-Navarro, Opt. Express **15,** 6750 (2007).
22. Q. Zhang, G. R. Chen, G. Zhang, J. R. Qiu, and D. P. Chen, J. Appl. Phys. **107,** 023102 (2010).
23. L. Zhang, J. Zhang, C. Yu, and L. Hu, J. Appl. Phys. **108,** 103117 (2010).
24. L. V. G. Tarelho, L. Gomes, and I. M. Ranieri, Phys. Rev. B **56,** 14344 (1997).
25. K. Li, Q. Zhang, G. Bai, S. Fan, J. Zhang, and L. Hu, J. Alloys and Compounds **504,** 573 (2010).
26. R. R. Xu, Y. Tian, M. Wang, L. L. Hu, and J. J. Zhang, Appl. Phys. B **102,** 109 (2011).
27. Y. S. Han, J. Heo, and Y. B. Shin, J. Non-Cryst. Solids **316,** 302 (2003).
28. A. Sennaroglu, A. Kurt, and G. Özen, J. Phys. **16,** 2471 (2004).
29. R. Balda, L. M. Lacha, J. Fernandez, and J. M. Fernandez-Navarro, Opt. Mater. **27,** 1771 (2005).